

# Mass and energy balance calculations for an artificial ice reservoir (Icestupa)

Suryanarayanan Balasubramanian<sup>1,\*</sup>, Martin Hoelzle<sup>1</sup>, Michael Lehning<sup>2</sup>,  
Sonam Wangchuk<sup>3</sup>, Johannes Oerlemans<sup>4</sup> and Felix Keller<sup>5</sup>

<sup>1</sup> University of Fribourg, Fribourg, Switzerland

<sup>2</sup> WSL Institute for Snow and Avalanche Research, Davos, Switzerland

<sup>3</sup> Himalayan Institute of Alternatives Ladakh, Leh, India

<sup>4</sup> Institute for Marine and Atmospheric Research, Utrecht University, Utrecht, The Netherlands

<sup>5</sup> Academia Engiadina, Samedan, Switzerland

Correspondence\*:

Suryanarayanan Balasubramanian

suryanarayanan.balasubramanian@unifr.ch

## 2 ABSTRACT

Artificial Ice Reservoirs (AIR) have been successful in storing water during winter and releasing the water during spring and summer. This has made them a reliable fresh water resource for irrigation in dry environments. Several AIRs have been built but studies of their water storage capacity and efficiency are scarce. This study attempts to model a cone-shaped AIR popularly called Icestupa. Important processes involved in the development and temporal evolution of an Icestupa are calculated by a physically-based model using equations governing the heat transfer, vapour diffusion and water transport of a phase changing water mass. These processes were quantified using meteorological data in conjunction with fountain spray information (mass input of an Icestupa) to estimate the quantity of frozen, melted, evaporated and drained water at a location called 'Eispalast' in the Schwarzsee region in the Canton of Fribourg, Switzerland. At this measurement site, an Icestupa was built for model validation purposes. The model was further tested by performing sensitivity and uncertainty study showing that the most sensitive parameters are the temperature threshold used to determine precipitation phase and the ice emissivity. Model calculations estimate that the Schwarzsee Icestupa only stored about 8% of the total water sprayed as ice. In addition, we found that reducing nozzle diameter of the fountain to 3 mm increases the storage efficiency up to 93% without compromising on the storage duration.

Keywords: iceslupa, mass balance, water storage, climate change adaptation, geoengineering

## 1 INTRODUCTION

Seasonal snow cover, glaciers and permafrost are expected to change their water storage capacity due to climate change with major consequences for downriver water supply (Immerzeel et al., 2019). The challenges brought about by these changes are especially important for dry mountain environments such as in Central Asia or the Andes, which directly rely on the seasonal meltwater for their farming and drinking needs (Hoelzle et al., 2019; Apel et al., 2018; Buytaert et al., 2017; Chen et al., 2016; Unger-Shayesteh

25 et al., 2013). Some villages in Ladakh, India have already been forced to relocate due to glacial retreat and  
26 the corresponding loss of their main fresh water resources (Grossman, 2015).

27 Artificial Ice Reservoirs (AIR) have been considered to be a feasible way to adapt to these changes  
28 (Hock et al., 2019; Nüsser et al., 2019b). An artificial ice reservoir is a human-made ice structure typically  
29 constructed during the cold winter months and designed to slowly release freshwater during the warm and  
30 dry spring and summer months. The main purpose of AIR is irrigation. Therefore, AIRs are designed to  
31 store water in the form of ice as long into the summer as possible. The energy required to construct an AIR  
32 is usually derived from the gravitational head of the source water body. Some are constructed horizontally  
33 by freezing water using a series of checkdams and others are built vertically by spraying water through  
34 fountain systems (Nüsser et al., 2019a). The latter are colloquially referred to as Icestupas and are the  
35 subject of this study.

36 Since their invention in 2013 (Wangchuk, 2014), Icestupas have gained widespread publicity in the region  
37 of Ladakh, Northern India since they require very little infrastructure, skills and energy to be constructed  
38 in comparison to other water storage technologies. Compared to other AIR geometries, Icestupas (Fig.  
39 1) can be built at lower altitudes and last much longer into the summer than other types of ice structures  
40 (Wangchuk, 2014).

41 If AIR are to become a viable water resource management tool, it is crucial to be able to propose suitable  
42 construction sites, and to identify and minimize water losses. However, to date, no reliable estimates exist  
43 about the amount of sprayed water that is necessary to create them and the meltwater they provide (Nüsser  
44 et al., 2019a). Rough estimates of Icestupa meltwater in Ladakh suggest that the water loss during the  
45 construction process is considerable (see Appendix 8.1). A complete set of measurements of the water  
46 storage and energy balance are urgently required to understand the cause of the water losses better and  
47 increase the construction efficiency.

48 In this paper, we aim to develop a physically-based model of a vertical AIR (or Icestupa) that can quantify  
49 their storage efficiency using existing weather and water usage information. Mass and energy balance  
50 equations were used to estimate the quantity of water frozen, melted, evaporated and wasted. Sensitivity  
51 and uncertainty analysis were performed to identify the most critical parameters and the variance caused  
52 by them. For validation, we created an Icestupa at an accessible site (called Eispalast) near Schwarzsee in  
53 the Canton of Fribourg, Switzerland, allowing easy maintenance and control of the measurements. Due  
54 to the low altitude of the site with relatively high winter temperatures, only a small Icestupa could be  
55 established during winter 2018/19 for providing us with model validation data. Our model and validation  
56 experiments provide first steps towards evaluating the effectiveness of a vertical AIR for irrigation and  
57 finally we outline some preliminary guidelines for consideration when a construction of an Icestupa for  
58 water storage is envisaged.

## 2 STUDY SITE

59 The 'Eispalast' site in the Schwarzsee region lies at 967 m a.s.l. In the winter (Oct-Mar), mean daily  
60 maximum and minimum air temperatures vary between 14 to -4 °C. Clear skies are rare, averaging around  
61 7 days, and precipitation amounts average 155 mm per month during winter (Meteoblue, 2020). The site  
62 was situated adjacent to a stream resulting in high humidity values across the study period. Within the  
63 'Eispalast' site, 1.8 m in radius enclosure was constructed for the experiment. An automatic weather station  
64 (AWS) was set in place adjacent to the wooden boundary as shown in Fig. 2. The fountain used for spraying  
65 water had a nozzle diameter of 5 mm and a height of 1.35 m, and was placed in the centre of the wooden  
66 enclosure. The water was transferred from a spring water source at 1267 m a.s.l. by pipeline and flowed



**Figure 1.** Icestupa in Ladakh, India on March 2017 was 24 m tall and contained around 3.7 million litres of water. Picture Credits: Lobzang Dadul

67 via a flowmeter and an air escape valve to the nozzle, where it was sprinkled with a spray radius of around  
 68 1.7 m. The air escape valve was installed to avoid errors in the flow measurements due to air bubbles. In  
 69 addition, a webcam guaranteed a continuous survey of the site during the construction of the Icestupa.

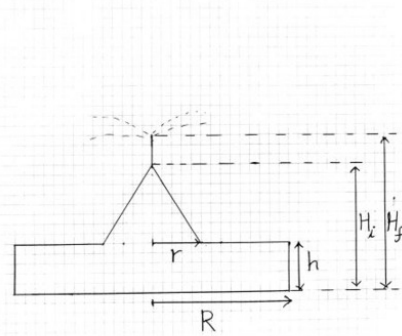


**Figure 2.** The ice structure during the first validation measurement as seen on the webcam image of 14<sup>th</sup> Feb. The corresponding cross section of the Schwarzesee ice structure with the field estimates of  $r$ ,  $R$ ,  $h$ ,  $H_i$ ,  $H_f$  used to determine the Icestupa volume is shown on the right.

## 70 2.1 Construction

71 From 30<sup>th</sup> January to 18<sup>th</sup> March 2019 the Icestupa was constructed through the fountain spray, which  
 72 was manually switched on if measured air temperature was below -5 °C after sunset and was switched  
 73 off as soon as the ice was exposed to daylight or temperatures were above 0 °C. The water spray of the  
 74 fountain was initially adjusted so that most of the water droplets land within the wooden boundary zone.  
 75 The ice formation was guided by adding a metal framework at the ice structure base after the first night of  
 76 operation. Several cotton threads were tied between the ice structure base and fountain pole for accelerating  
 77 and further guiding the ice formation process.

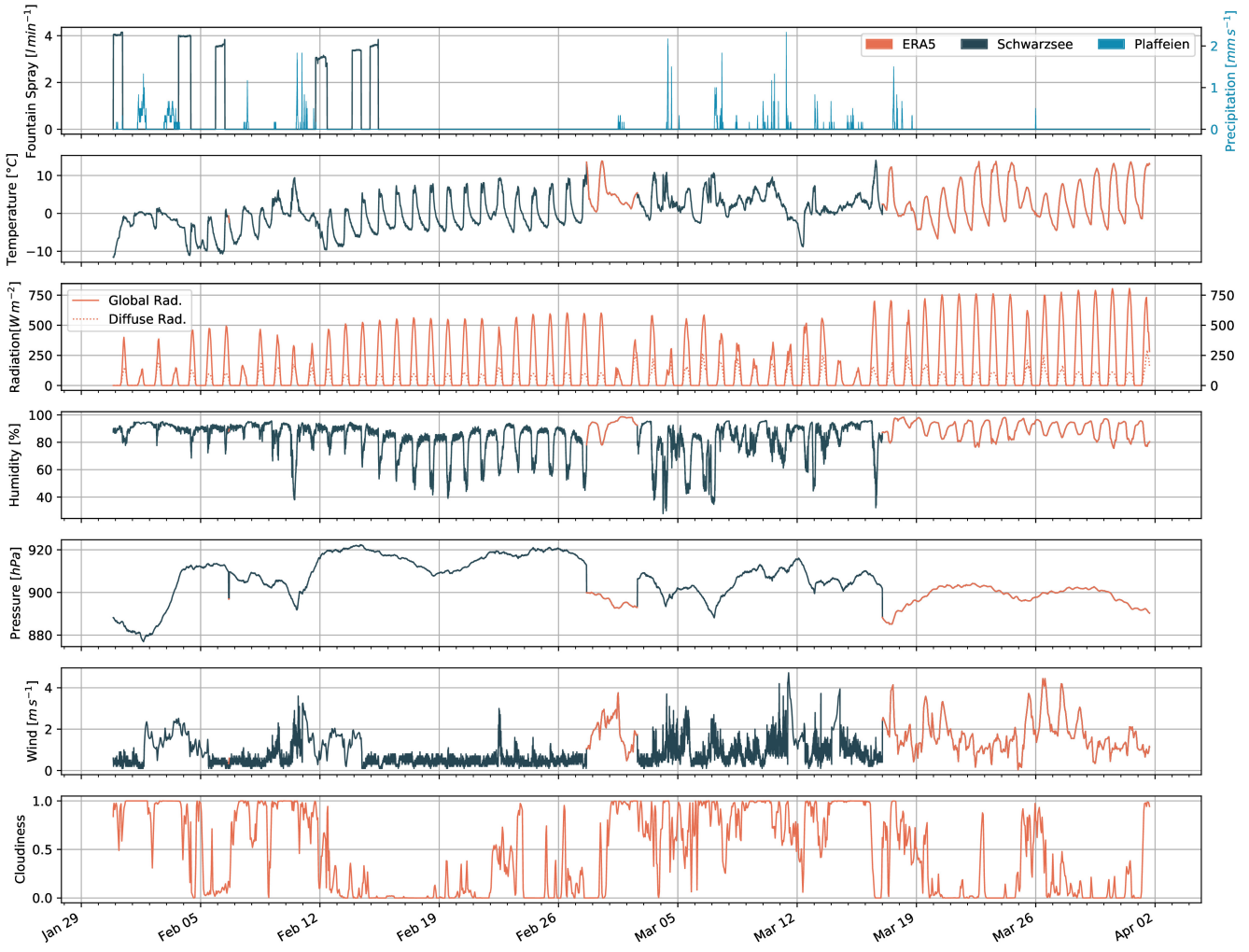


**Figure 3.** Measurements at the AWS of Schwarzsee were used as main model input data in 5 minute frequency. Plaffeien AWS provided the precipitation data. Cloudiness and incoming shortwave radiation were obtained from the ERA5 reanalysis dataset.

## 78 2.2 Measurements and Data

79 The Schwarzsee AWS was located at 967 m a.s.l. It was in operation from 30<sup>th</sup> January to 18<sup>th</sup> March  
 80 2019. Measurements comprise air temperature, relative humidity, water flow, wind speed and direction.  
 81 All these measurements were stored as 5 minute means. Precipitation data was derived from the Plaffeien  
 82 AWS (IDAWEB, 2019) located 8.8 km away from the measurement site at an altitude of 1042 m a.s.l. In  
 83 order to acquire cloudiness and incoming shortwave radiation data, we used the ERA5 reanalysis dataset at  
 84 Schwarzsee (Copernicus Climate Change Service (C3S), 2017). The hourly ERA5 data and the 10 minute  
 85 Plaffeien AWS data were linearly interpolated to the 5 minute data frequency of the Schwarzsee AWS.

86 Due to a power failure, all data from the Schwarzsee AWS was lost between 27<sup>th</sup> February 15:20 to 2<sup>nd</sup>  
 87 March 15:00. Consequently, the amount of missing data in the dataset was around 6.7%. During heavy  
 88 snowfall events, the ultrasonic wind sensor was blocked and recorded zero values. These data gaps and  
 89 errors were filled with the Plaffeien AWS precipitation and ERA5 reanalysis dataset. ERA5 air temperature  
 90 was found to be highly correlated ( $r^2 = 0.85$ ) with the Schwarzsee dataset but the corresponding wind

speed values were poorly correlated ( $r^2 = 0.18$ ). However, in a second step, we further extended the dataset beyond 18<sup>th</sup> March 2019 (Fig. 3) to enable the model to completely melt the Icestupa.

### 2.2.1 Field Measurements for validation

Estimates of the ice volumes were obtained by two manual measurements of the ice structure dimensions. The first corresponds to the end of the freezing period on 14<sup>th</sup> February 16:00 (only one more fountain run was possible after this date). The second corresponds to the end of the melting process on 10<sup>th</sup> March 18:00. The field validations are shown by green lines in Fig. 8.

On 14<sup>th</sup> February the ice volume was calculated using a simplistic cross section of the structure as shown in Fig. 2. We used the following field estimates of  $r, R, h, H_i, H_f$  (see Fig. 2 for the different geometry components) to determine the maximum and minimum volumes:

$$0.55 \leq r \leq 1m ; 1.1 \leq R \leq 1.2m ; 0.1 \leq h \leq 0.2m ; 0.6 \leq H_i \leq 0.8m ; 1.3 \leq H_f \leq 1.4m \quad (1)$$

The second validation point was considered to be on March 10<sup>th</sup> 18:00. Based on the webcam imagery and manual measurement, a thin layer of ice with an observed thickness between 0.01 to 0.06 m could be quantified. This results in an ice volume estimate for the first validation date on 14<sup>th</sup> February 2019 to be  $0.857 \pm 0.186 m^3$  and for the second validation date on 11<sup>th</sup> March 2019 to be  $0.13 \pm 0.09 m^3$ .

In reality, the Schwarzsee ice structure was more cylindrical until a height of 0.2 m and conical afterwards until a height of 0.6 m with a radius of 1.18 m. However, we assume a conical shape of this ice structure in order to apply the modelling strategy described below.

## 3 MODEL SETUP

The model (implemented in python) consists of three parts calculating a) the geometric evolution of the Icestupa, b) the energy balance and c) the mass balance as shown schematically in Fig. 4. A bulk energy and mass balance model is used to calculate the amounts of ice, liquid water, water vapour and drained water of the Icestupa every 5 minutes. The equations used henceforth display model time step superscript only if it is different from the current time step.

### 3.1 Icestupa geometric evolution

Radius  $r_{ice}$  and height  $h_{ice}$  define the dimensions of the Icestupa assuming its geometry to be a cone as shown in Fig. 5. The surface area  $A$  and volume  $V$  exposed to the atmosphere are:

$$A = \pi \cdot r_{ice} \cdot \sqrt{r_{ice}^2 + h_{ice}^2} \quad (2)$$

$$V = \pi/3 \cdot r_{ice}^2 \cdot h_{ice} \quad (3)$$

With the mass of the Icestupa  $M_{ice}$ , its current volume can also be expressed as:

$$V = M_{ice}/\rho_{ice} \quad (4)$$

where  $\rho_{ice}$  is the density of ice ( $917 kg m^{-3}$ ). The model of the Icestupa is initialised with a thickness of  $\Delta x$  (defined in 3.2) and a circular area of radius  $r_F$ . The constant  $r_F$  represents the mean spray radius

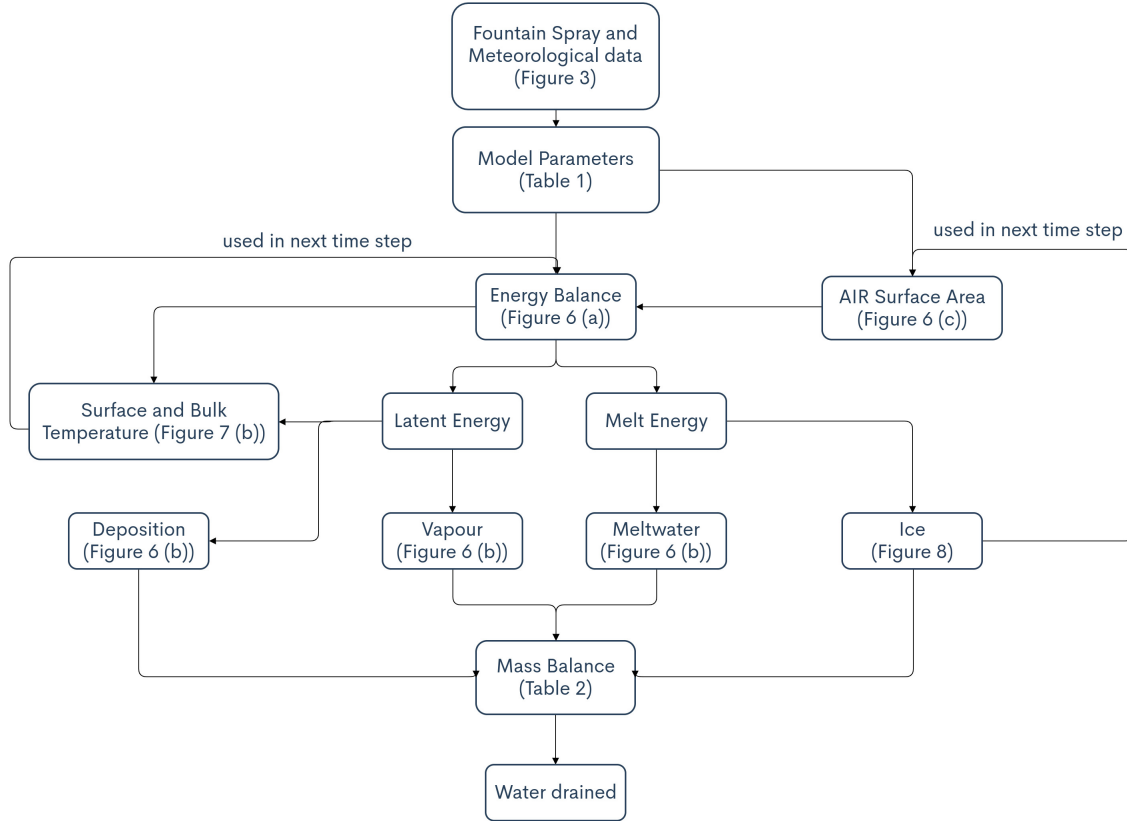


**Figure 4.** Model schematic showing the algorithm used in the model at every time step. Further details about these variables can be found in the associated tables and figures.

119 of the fountain. This fountain spray radius is determined by modelling the projectile motion of the water  
120 droplets. Using mass conservation the droplet speed  $v_F$  can be determined from the spray rate  $d_F$  and the  
121 diameter  $dia_F$  of the nozzle as follows:

$$v_F = \frac{d_F}{\pi \cdot dia_F^2 / 4} \quad (5)$$

122 Afterwards, we assume that the water droplets move with an air friction free projectile motion from  
123 the fountain nozzle with a height  $h_F$  to the ice/ground surface. The resulting spray radius  $r_F$  was then  
124 determined from the projectile motion equation as follows:

$$r_F = \frac{v_F \cdot \cos\theta_F (v_F \cdot \sin\theta_F + \sqrt{(v_F \cdot \sin\theta_F)^2 + 2 \cdot g \cdot h_F})}{g} \quad (6)$$

125 where  $g = 9.8ms^{-2}$  is the acceleration due to gravity and  $\theta_F = 45^\circ$  is the angle of launch.

126 During subsequent time steps, the dimensions of the Icestupa evolve assuming a uniform ice formation  
127 and decay across its surface area with an invariant slope  $s_{cone} = \frac{h_{ice}}{r_{ice}}$  as shown in Fig. 5. During these time  
128 steps, the volume is parameterised using Eqn. 3 as:

$$V = \pi/3 \cdot r_{ice}^3 \cdot s_{cone} \quad (7)$$

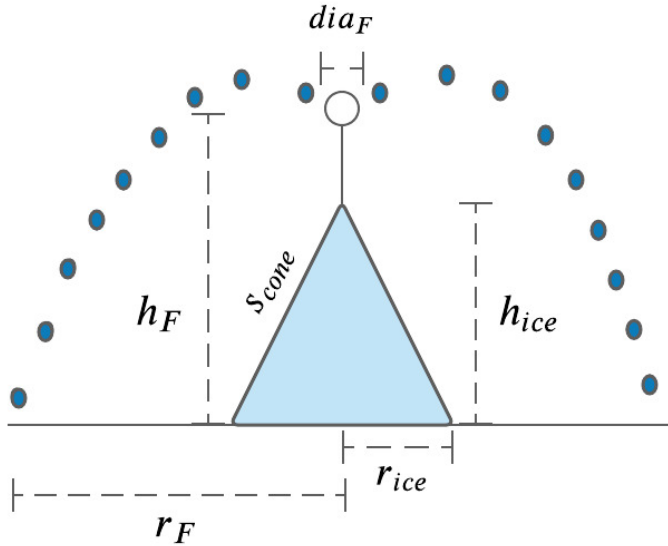


**Figure 5.** Shape and fountain parameters of the Schwarzsee Icestupa.  $r_{ice}$  is the radius,  $h_{ice}$  is the height and  $s_{cone}$  is the slope of the ice cone.  $r_F$  is the spray radius,  $h_F$  is the height and  $dia_F$  is the nozzle diameter of the fountain.

129 However, the Icestupa cannot outgrow the maximum range of the water droplets ( $(r_{ice})_{max} = r_F$ ).  
 130 Combining equations 3, 4 and 7, the geometric evolution of the Icestupa at each time step  $i$  can be  
 131 determined by considering the following rules:

$$(r_{ice}, h_{ice}) = \begin{cases} (r_F, \Delta x) & \text{if } i = 0 \\ (r_{ice}^{i-1}, \frac{3 \cdot M_{ice}}{\pi \cdot \rho_{ice} \cdot (r_{ice}^{i-1})^2}) & \text{if } r_{ice}^{i-1} \geq r_F \text{ and } \Delta M_{ice} > 0 \text{ where } \Delta M_{ice} = M_{ice}^{i-1} - M_{ice}^{i-2} \\ (\frac{3 \cdot M_{ice}}{\pi \cdot \rho_{ice} \cdot s_{cone}})^{1/3} \cdot (1, s_{cone}) & \text{otherwise} \end{cases} \quad (8)$$

### 132 3.2 Energy Balance

133 The energy balance equation for the Icestupa is formulated as follows:

$$q_{net} = q_{SW} + q_{LW} + q_L + q_S + q_F + q_G \quad (9)$$

134 where  $q_{net}$  is the net energy flux in  $[W m^{-2}]$ ;  $q_{SW}$  is the net shortwave radiation;  $q_{LW}$  is the net longwave  
 135 radiation;  $q_L$  and  $q_S$  are the turbulent latent and sensible heat fluxes.  $q_F$  represents the heat exchange  
 136 created due to the additional water and ice boundary present during fountain on time steps.  $q_G$  represents  
 137 ground heat flux between Icestupa surface and Icestupa interior. Energy transferred in the direction of the  
 138 ice surface is always denoted as positive and away as negative. Also, all temperature variables are assigned  
 139 in units of  $^{\circ}C$ .

140 Equation 9 is usually referred to as the energy budget for “the surface”, but practically it must apply to a  
 141 surface layer of ice with a finite thickness  $\Delta x$ . The energy flux acts upon the Icestupa surface layer which

142 has an upper and a lower boundary defined by the atmosphere and the ice body of the Icestupa, respectively.  
 143 The parameter selection for  $\Delta x$  is based on the following two arguments: (a) the ice thickness  $\Delta x$  should  
 144 be small enough to represent the daily surface temperature variations and (b)  $\Delta x$  should be large enough  
 145 for these temperature variations to not reach the bottom of the surface layer. Therefore, we introduced a 5  
 146 mm thick ice surface layer, over which the energy balance is calculated. A sensitivity analysis was later  
 147 performed to understand the influence of this factor. Here, we define the surface temperature  $T_{ice}$  to be  
 148 the modelled average temperature of the Icestupa surface layer and the energy flux  $q_{net}$  is assumed to act  
 149 uniformly across the Icestupa area  $A$ .

### 150 3.2.1 Net Shortwave Radiation $q_{SW}$

151 The net shortwave radiation  $q_{SW}$  is computed as follows:

$$q_{SW} = (1 - \alpha) \cdot (SW_{direct} \cdot f_{cone} + SW_{diffuse}) \quad (10)$$

152 where  $SW_{direct} = SW_{global} - SW_{diffuse}$  with the measured global and diffuse short wave radiation as  
 153  $SW_{global}$  and  $SW_{diffuse}$ , the modelled albedo as  $\alpha$  and with  $f_{cone}$  as the area fraction of the ice structure  
 154 exposed to the direct shortwave radiation.

155 We model the albedo using a scheme described in Oerlemans and Knap (1998). The scheme records the  
 156 decay of albedo with time after fresh snow is deposited on the surface.  $\delta t$  records the number of time steps  
 157 after the last snowfall event. After snowfall, albedo changes over a time step,  $\delta t$ , as

$$\alpha = \alpha_{ice} + (\alpha_{snow} - \alpha_{ice}) \cdot e^{(-\delta t)/\tau} \quad (11)$$

158 where  $\alpha_{ice}$  is the bare ice albedo value and  $\tau$  is a decay rate, which determines how fast the albedo of the  
 159 ageing snow reaches this value. The decay rate  $\tau$  is assumed to have a base value of 10 days similar to  
 160 values obtained by Schmidt et al. (2017) for wet surfaces and its maximal value is set based on observations  
 161 by Oerlemans and Knap (1998) as shown in Table 1. Furthermore, the albedo  $\alpha$  varies depending on the  
 162 water source that formed the current Icestupa surface. Correspondingly, the albedo is reset to the value  
 163 of bare ice albedo if the fountain is spraying water onto the current ice surface and to the value of fresh  
 164 snow albedo if a snowfall event occurred. Snowfall events are assumed if the air temperature is below  
 165  $T_{rain} = 1^{\circ}C$ .

166 The area fraction  $f_{cone}$  of the ice structure exposed to the direct shortwave radiation depends on the  
 167 shape considered. This factor is derived by calculating the area influenced by the vertical and horizontal  
 168 components of the direct solar radiation. For a conical shape, half of the total curved surface is exposed to  
 169 the vertical component of the direct shortwave radiation and the projected triangle of the curved surface  
 170 is exposed to the horizontal component of the direct shortwave radiation. The solar elevation angle  $\theta_{sun}$   
 171 used is modelled using the parametrisation proposed by Woolf (1968). Accordingly,  $f_{cone}$  is determined as  
 172 follows:

$$f_{cone} = \frac{(0.5 \cdot r_{ice} \cdot h_{ice}) \cdot \cos\theta_{sun} + (\pi \cdot r_{ice}^2 / 2) \cdot \sin\theta_{sun}}{\pi \cdot r_{ice} \cdot (r_{ice}^2 + h_{ice}^2)^{1/2}} \quad (12)$$

173 The measured diffuse shortwave radiation is assumed to impact the conical Icestupa surface uniformly.

174 3.2.2 Net Longwave Radiation  $q_{LW}$ 

175 The net longwave radiation  $q_{LW}$ , for which there were no direct measurements available at Schwarzsee,  
 176 is determined as follows:

$$177 \quad q_{LW} = \sigma \cdot (\epsilon_a \cdot (T_a + 273.15)^4 - \epsilon_{ice} \cdot (T_{ice} + 273.15)^4) \quad (13)$$

177 where  $T_a$  represents the measured air temperature,  $T_{ice}$  is the modelled surface temperature, both  
 178 temperatures are given in  $^{\circ}\text{C}$ ,  $\sigma = 5.67 \cdot 10^8$  is the Stefan-Boltzmann constant,  $\epsilon_a$  denotes the atmospheric  
 179 emissivity and  $\epsilon_{ice}$  is the corresponding emissivity value for the Icestupa surface (see Table 1).

180 For the calculation of the incoming longwave radiation, we approximate atmospheric emissivity  $\epsilon_a$  using  
 181 the equation suggested by Brutsaert (1982), considering air temperature and vapor pressure (Eqn. 15). The  
 182 vapor pressures over air and ice was obtained using the following formulation given in WMO (2018):

$$183 \quad p_{v,a} = 6.107 \cdot 10^{(7.5 \cdot T_a / (T_a + 237.3))} \\ p_{v,ice} = (1.0016 + 3.15 \cdot 10^{-6} \cdot p_a - 0.074 \cdot p_a^{-1}) \cdot (6.112 \cdot e^{(22.46 \cdot T_{ice} / (T_{ice} + 272.62))}) \quad (14)$$

183 where  $p_{v,a}$  denotes the saturation vapor pressure of air,  $p_{v,ice}$  denotes the saturation vapor pressure of ice  
 184 and  $p_a$  is the measured air pressure in  $[hPa]$ . The expression defined in Brutsaert (1975) for clear skies  
 185 (first term in equation 15) is extended with the correction for cloudy skies after Brutsaert (1982) as follows:

$$186 \quad \epsilon_a = 1.24 \cdot \left( \frac{p_{v,a}}{(T_a + 273.15)} \right)^{1/7} \cdot (1 + 0.22 \cdot c^2) \quad (15)$$

186 with a cloudiness index  $c$ , ranging from 0 for clear skies to 1 for complete overcast skies, obtained from  
 187 the ERA5 reanalysis data as shown in Fig. 3.

188 3.2.3 Turbulent sensible  $q_S$  and latent  $q_L$  heat fluxes

189 The turbulent sensible  $q_S$  and latent heat  $q_L$  fluxes are computed with the following expressions proposed  
 190 by Garratt (1992):

$$191 \quad q_S = c_a \cdot \rho_a \cdot p_a / p_{0,a} \cdot \frac{\kappa^2 \cdot v_a \cdot (T_a - T_{ice})}{(\ln \frac{h_{AWS}}{z_{ice}})^2} \quad (16)$$

$$192 \quad q_L = \begin{cases} 0.623 \cdot L_s \cdot \rho_a / p_{0,a} \cdot \frac{\kappa^2 \cdot v_a (p_{v,a} - p_{v,ice})}{(\ln \frac{h_{AWS}}{z_{ice}})^2} & \text{if } \Delta M_F = 0 \\ 0 & \text{if } \Delta M_F > 0 \text{ where } \Delta M_F = M_F^i - M_F^{i-1} \end{cases} \quad (17)$$

191 where  $h_{AWS}$  is the measurement height above the ground surface of the AWS (in  $m$ ),  $v_a$  is the wind  
 192 speed in  $[m s^{-1}]$  and  $M_F$  denotes fountain water spray mass in  $[kg]$ .  $c_a$  is the specific heat of air at constant  
 193 pressure ( $1010 \text{ J kg}^{-1} K^{-1}$ ),  $\rho_a$  is the air density at standard sea level ( $1.29 \text{ kg m}^{-3}$ ),  $p_{0,a}$  is the air pressure  
 194 at standard sea level ( $1013 \text{ hPa}$ ),  $\kappa$  is the von Karman constant (0.4),  $L_s$  is the heat of sublimation (2848  
 195  $\text{kJ kg}^{-1}$ ) and  $z_{ice}$  (1.7 mm) denotes the roughness length of ice (momentum and scalar).

196 3.2.4 Fountain water heat flux  $q_F$

197 The total energy flux is further influenced through the heat flux caused by the water that was additionally  
 198 added to the surface of the Icestupa during the time the fountain was running. We take this interaction  
 199 between the fountain water and the ice surface into account by assuming that the ice surface temperature  
 200 stays constantly at  $0^\circ C$  during time steps when the fountain is active. This process can be divided into two  
 201 simultaneous steps: (a) the water temperature  $T_{water}$  is cooled to  $0^\circ C$  and (b) the ice surface temperature is  
 202 warmed to  $0^\circ C$ . Process (a) transfers hereby the necessary energy for process (b) throughout the fountain  
 203 runtime. We further assume that this process is instantaneous, i.e. the ice temperature is immediately set  
 204 to  $0^\circ C$  within just one time step  $\Delta t$  when the fountain is switched on. Thus, the heat flux caused by the  
 205 fountain water is calculated as follows:

$$q_F = \begin{cases} 0 & \text{if } \Delta M_F = 0 \\ \frac{\Delta M_F \cdot c_{water} \cdot T_{water}}{\Delta t \cdot A} + \frac{\rho_{ice} \cdot \Delta x \cdot c_{ice} \cdot T_{ice}}{\Delta t} & \text{if } \Delta M_F > 0 \end{cases} \quad (18)$$

206 with  $c_{ice}$  as the specific heat of ice.

207 3.2.5 Bulk Icestupa heat flux  $q_G$

208 The bulk Icestupa heat flux  $q_G$  corresponds to the ground heat flux in normal soils and is caused by  
 209 the temperature gradient between the surface layer and the ice body. It is expressed by using the heat  
 210 conduction equation as follows:

$$q_G = k_{ice} \cdot (T_{bulk} - T_{ice}) / l_{ice} \quad (19)$$

211 where  $k_{ice}$  is the thermal conductivity of ice in  $[W\ m^{-1}\ K^{-1}]$ ,  $T_{bulk}$  is the mean temperature of the ice  
 212 body within the Icestupa and  $l_{ice}$  is the average distance of any point in the surface to any other point in the  
 213 ice body.  $T_{bulk}$  is initialised as  $0^\circ C$  and later determined from Eqn. 19 as follows:

$$T_{bulk} = T_{bulk}^{i-1} - (q_G \cdot A \cdot \Delta t) / (M_{ice} \cdot c_{ice}) \quad (20)$$

214 Since we assume a conical shape with  $r_{ice} > h_{ice}$ ,  $l_{ice}$  cannot be greater than  $2r_{ice}$  and also cannot  
 215 be less than  $\Delta x$ . Therefore, the average distance from any point on the surface to any point inside is  
 216  $\Delta x \leq l_{ice} \leq r_{ice}$ . We calculate  $q_G$  here assuming  $l_{ice} = r_{ice}/2$ .

217 3.2.6 Surface temperature changes and melt energy  $q_{melt}$

218 The available net energy  $q_{net}$  partly increases surface temperature, but also contributes to ice melt at the  
 219 surface of the Icestupa.  $q_T$  denotes the energy used on changing the surface temperature  $T_{ice}$  and  $q_{melt}$   
 220 denotes the energy used to produce meltwater. So Eqn. 9 can be rewritten as:

$$q_{net} = q_{melt} + q_T \quad (21)$$

221 The temperature fluctuates based on 3 scenarios namely, (a) the energy flux is negative but cannot freeze  
 222 all the fountain water output; (b) the energy flux is negative and can freeze all the fountain water output and  
 223 (c) the fountain is inactive ( $\Delta M_F = 0$ ). Also, the latent heat always contributes to temperature fluctuations.  
 224 Therefore, we express the rate of change of temperature as follows:

$$\frac{\Delta T}{\Delta t} = \begin{cases} -T_{ice}^{i-1}/\Delta t & \text{if } (q_{net} - q_L) < 0 \text{ and } \Delta M_F \geq -(q_{net} - q_L) \cdot A \cdot \Delta t / L_f \\ (\Delta M_F \cdot L_f) / (\rho_{ice} \cdot c_{ice} \cdot \Delta x \cdot A \cdot \Delta t) & \text{if } (q_{net} - q_L) < 0 \text{ and } \Delta M_F < -(q_{net} - q_L) \cdot A \cdot \Delta t / L_f \\ q_{net} / (\rho_{ice} \cdot c_{ice} \cdot \Delta x) & \text{if } \Delta M_F = 0 \end{cases} \quad (22)$$

225 Whenever the model predicts  $T_{ice}^{i+1} > 0^\circ C$ , then the surface temperature is set to  $0^\circ C$  in the corresponding  
 226 time step and additional energy contributes to  $q_{melt}$ . Combining these requirements, we get:

$$(q_T, q_{melt}) = \begin{cases} (\rho_{ice} \cdot c_{ice} \cdot \Delta x \cdot \frac{\Delta T}{\Delta t}, q_{net} - q_L - \rho_{ice} \cdot c_{ice} \cdot \Delta x \cdot \frac{\Delta T}{\Delta t}) & \text{if } T_{ice}^{i+1} \leq 0 \text{ and } \Delta M_F > 0 \\ (\rho_{ice} \cdot c_{ice} \cdot \Delta x \cdot \frac{\Delta T}{\Delta t}, q_{net} - \rho_{ice} \cdot c_{ice} \cdot \Delta x \cdot \frac{\Delta T}{\Delta t}) & \text{if } T_{ice}^{i+1} \leq 0 \text{ and } \Delta M_F = 0 \\ (-\rho_{ice} \cdot c_{ice} \cdot \Delta x \cdot \frac{T_{ice}^i}{\Delta t}, q_{net} - q_L + \rho_{ice} \cdot c_{ice} \cdot \Delta x \cdot \frac{T_{ice}^i}{\Delta t}) & \text{if } T_{ice}^{i+1} > 0 \text{ and } \Delta M_F > 0 \\ (-\rho_{ice} \cdot c_{ice} \cdot \Delta x \cdot \frac{T_{ice}^i}{\Delta t}, q_{net} + \rho_{ice} \cdot c_{ice} \cdot \Delta x \cdot \frac{T_{ice}^i}{\Delta t}) & \text{if } T_{ice}^{i+1} > 0 \text{ and } \Delta M_F = 0 \end{cases} \quad (23)$$

**Table 1.** Free parameters in the model categorised as constant, uncertain and site parameters. Base value (B) and uncertainty (U) were taken from the literature. For assumptions (assum.), the uncertainty was chosen to be relatively large (5 %). For measurements (meas.), the uncertainty due to parallax errors is chosen to be (1 %).

Constant Parameters	Symbol	Value	Range	References
Van Karman constant	$\kappa$	0.4	n.a.	B: Cuffey and Paterson
Stefan Boltzmann constant	$\sigma$	$5.67 \cdot 10^{-8} W m^{-2} K^{-4}$	n.a.	B: Cuffey and Paterson
Air pressure at sea level	$p_{0,a}$	1013 hPa	n.a.	B: Mölg and Hardy
Density of water	$\rho_w$	$1000 kg m^{-3}$	n.a.	B: Cuffey and Paterson
Density of ice	$\rho_{ice}$	$917 kg m^{-3}$	n.a.	B: Cuffey and Paterson
Density of air	$\rho_a$	$1.29 kg m^{-3}$	n.a.	B: Mölg and Hardy
Specific heat of water	$c_w$	$4186 J kg^{-1} ^\circ C^{-1}$	n.a.	B: Cuffey and Paterson
Specific heat of ice	$c_{ice}$	$2097 J kg^{-1} ^\circ C^{-1}$	n.a.	B: Cuffey and Paterson
Specific heat of air	$c_a$	$1010 J kg^{-1} ^\circ C^{-1}$	n.a.	B: Mölg and Hardy
Thermal conductivity of ice	$k_{ice}$	$2.123 W m^{-1} K^{-1}$	n.a.	B: Bonales et al.
Latent Heat of Sublimation	$L_s$	$2848 kJ kg^{-1}$	n.a.	B: Cuffey and Paterson
Latent Heat of Evaporation	$L_e$	$2514 kJ kg^{-1}$	n.a.	B: Cuffey and Paterson
Latent Heat of Fusion	$L_f$	$334 kJ kg^{-1}$	n.a.	B: Cuffey and Paterson
Gravitational acceleration	$g$	$9.81 m s^{-2}$	n.a.	B: Cuffey and Paterson
<hr/>				
Uncertain Parameters				
Precipitation Temperature threshold	$T_{rain}$	$1 ^\circ C$	$\pm 1 ^\circ C$	B + U: Fujita and Ageta, Zhou et al.
Ice Emissivity	$\epsilon_{ice}$	0.95	$\pm 5 \%$	B: Cuffey and Paterson; U: assum.
Ice Albedo	$\alpha_{ice}$	0.35	$\pm 5 \%$	B: Cuffey and Paterson; U: assum.
Snow Albedo	$\alpha_{snow}$	0.85	$\pm 5 \%$	B: Cuffey and Paterson; U: assum.
Albedo Decay Rate	$\tau$	10 days	[1, 22] days	B: Schmidt et al.; U: Oerlemans and Knap
Ice layer thickness	$\Delta x$	5 mm	[1, 10] mm	assum.
<hr/>				
Site Parameters				
Fountain nozzle diameter	$dia_F$	5 mm	$\pm 1 \%$	B: meas. ; U: assum.
Fountain Height	$h_F$	1.35 m	$\pm 1 \%$	B: meas. ; U: assum.
Fountain water temperature	$T_{water}$	5 °C	[0, 9] °C	B: meas. ; U: meas.
AWS Height	$h_{AWS}$	3 m	$\pm 1 \%$	B: meas. ; U: assum.

$$M_F + M_{ppt} + M_{dpt} = M_{ice} + M_{melt} + M_{vapour} + M_{drained} \quad (24)$$

227 where  $M_F$  denotes the cumulative water input;  $M_{ppt}$  is the cumulative precipitation and  $M_{dpt}$  is the  
 228 cumulative accumulation through water vapour condensation or deposition;  $M_{ice}$  is the cumulative mass of  
 229 ice;  $M_{melt}$  is the cumulative mass of melt water;  $M_{vapour}$  represents the cumulative water vapor loss by  
 230 evaporation or sublimation and  $M_{drained}$  is the cumulative water that drains away.

231 Equation 24 can be rewritten using the mass balance change as:

$$\frac{\Delta M_F}{\Delta t} + \frac{\Delta M_{ppt}}{\Delta t} + \frac{\Delta M_{dpt}}{\Delta t} = \frac{\Delta M_{ice}}{\Delta t} + \frac{\Delta M_{melt}}{\Delta t} + \frac{\Delta M_{vapour}}{\Delta t} + \frac{\Delta M_{drained}}{\Delta t} \quad (25)$$

232 where  $\Delta M = M^i - M^{i-1}$ . Here  $\frac{\Delta M_F}{\Delta t} = d_F$  where  $d_F$  is the spray of the fountain measured in  $[kg s^{-1}]$ .  
 233 Precipitation input is calculated as:

$$\frac{\Delta M_{ppt}}{\Delta t} = \begin{cases} \pi \cdot r_{ice}^2 \cdot \rho_w \cdot ppt & \text{if } T_a < T_{rain} \\ 0 & \text{if } T_a \geq T_{rain} \end{cases} \quad (26)$$

234 where  $\rho_w$  is the density of water ( $1000 kg m^{-3}$ ),  $ppt$  is the measured precipitation rate in  $[m s^{-1}]$  and  
 235  $T_{rain}$  is the temperature threshold below which precipitation falls as snow. Here, snowfall events were  
 236 identified using  $T_{rain}$  as  $1^\circ C$ . Snow mass input is calculated by assuming a uniform deposition over the  
 237 entire circular footprint of the Icestupa.

238 The latent heat energy is used to estimate either the evaporation and condensation processes or sublimation  
 239 and deposition processes. Deposition and sublimation involve phase change between vapour and ice  
 240 whereas evaporation and condensation involve phase change between meltwater and ice. To differentiate  
 241 between these two possibilities, we classify the time steps into humid or non-humid if the corresponding  
 242 relative humidity value is above or below 60 % (Stigter et al., 2018). On humid time steps we assume  
 243 condensation or evaporation to occur whereas on non-humid time steps deposition or sublimation can occur.  
 244 Correspondingly, latent heat of evaporation ( $L_e$ ) is used for humid time steps and latent heat of sublimation  
 245 ( $L_s$ ) is used for non-humid time steps. Water accumulation and vapour loss from the Icestupa surface is  
 246 calculated as follows:

$$\left( \frac{\Delta M_{vapour}}{\Delta t}, \frac{\Delta M_{dpt}}{\Delta t} \right) = \begin{cases} (q_L \cdot A/L, 0) & \text{if } q_L < 0 \\ (0, -q_L \cdot A/L) & \text{if } q_L \geq 0 \end{cases} \quad (27)$$

247 where  $L = \begin{cases} L_e & \text{if } RH \geq 60 \\ L_s & \text{if } RH < 60 \end{cases}$

248 Using the melt energy  $q_{melt}$ , we estimate the frozen and melted ice mass ( $\Delta M_{ice}$ ,  $\Delta M_{melt}$ ). Removing  
 249 the contribution of precipitation and combining Eqn. 27 we are left with the contribution from the melt  
 250 energy as follows:

**Table 2.** Summary of calculated mass balance components for the Schwarzsee experiment after the fountain spray was stopped on 15<sup>th</sup> February and at the end of the model run on 1<sup>st</sup> April.

	Mass Component	Fountain spray ends	Model ends
Input	$M_F$	18060 kg	18060 kg
	$M_{ppt}$	439 kg	463 kg
	$M_{dpt}$	14 kg	62 kg
Output	$M_{melt}$	166 kg	1392 kg
	$M_{ice}$	1158 kg	0 kg
	$M_{vapour}$	4 kg	8 kg
	$M_{drained}$	17184 kg	17184 kg

$$\left( \frac{\Delta M_{ice} - \Delta M_{ppt} - \Delta M_{dpt} + \Delta M_{vapour}}{\Delta t}, \frac{\Delta M_{melt}}{\Delta t} \right) \begin{cases} \text{if } RH \leq 60 \\ \left( \frac{\Delta M_{ice} - \Delta M_{ppt} - \Delta M_{dpt}}{\Delta t}, \frac{\Delta M_{melt} + \Delta M_{vapour}}{\Delta t} \right) \begin{cases} \frac{q_{melt} \cdot A}{L_f} \cdot (-1, 1) & \text{if } q_{melt} \geq 0 \\ \frac{q_{melt} \cdot A}{L_f} \cdot (-1, 0) & \text{if } q_{melt} < 0 \text{ and } \frac{\Delta M_F}{\Delta t} \geq -q_{melt} \\ (\frac{\Delta M_F}{\Delta t}, 0) & \text{if } q_{melt} < 0 \text{ and } 0 \leq \frac{\Delta M_F}{\Delta t} < -q_{melt} \end{cases} \end{cases} \quad (28)$$

251 Now, with all the other terms known in Eqn. 25, the water drained from the Icestupa can be expressed as:

$$\frac{\Delta M_{drained}}{\Delta t} = \frac{\Delta M_F + \Delta M_{ppt} + \Delta M_{dpt} - \Delta M_{ice} - \Delta M_{melt} - \Delta M_{vapour}}{\Delta t} \quad (29)$$

252 Considering AIR as water reservoirs, we can quantify their potential through the amount of water they  
253 store (storage quantity) and the length of time they store it (storage duration). Another means of comparing  
254 different Icestupas is through their water storage efficiency defined accordingly as:

$$\text{Storage Efficiency} = \frac{M_{melt}}{(M_F + M_{ppt} + M_{dpt})} \cdot 100 \quad (30)$$

## 4 MODEL RESULTS

255 The model was forced with meteorological data from 30<sup>th</sup> January to 1<sup>st</sup> April 2019 (Fig. 3) and various  
256 parameters (see Table 1) to calculate the mass and energy balance of the Icestupa.

### 257 4.1 Energy and mass balance calculation

258 Daily averages of some components of the energy balance are shown in Fig. 6 (a). On average during the  
259 experiment duration, the total energy flux between the atmosphere and the Icestupa are almost balanced.  
260 Net shortwave radiation ( $28 \text{ W m}^{-2}$ ), sensible ( $17 \text{ W m}^{-2}$ ) and latent heat flux ( $9 \text{ W m}^{-2}$ ) with a mostly

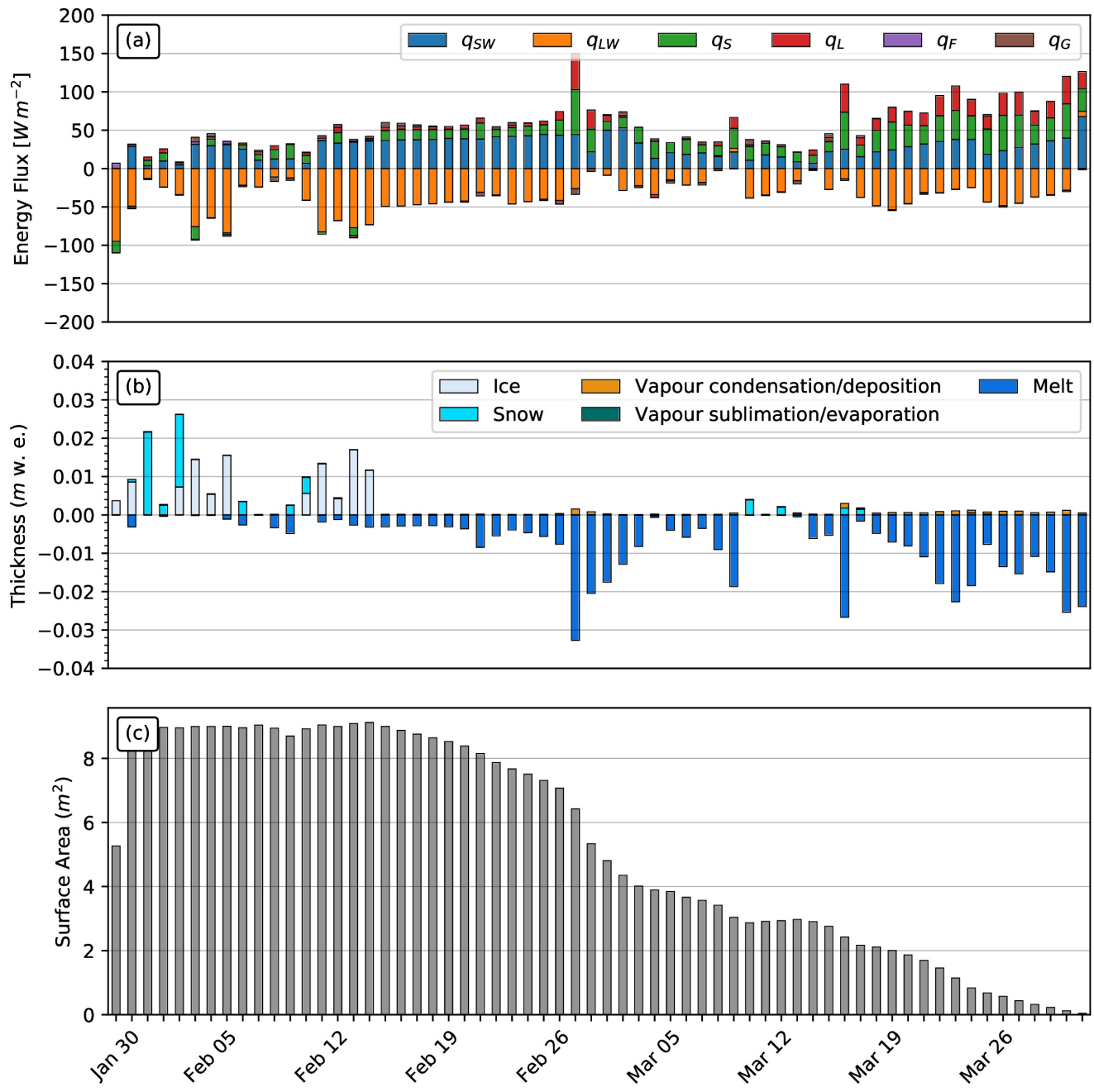


**Figure 6.** (a) Energy flux components, (b) mass flux components and (c) surface area of the Icestupa in daily time steps.  $q_{SW}$  is the net shortwave radiation;  $q_{LW}$  is the net longwave radiation;  $q_L$  and  $q_S$  are the turbulent latent and sensible heat fluxes.  $q_F$  represents the interactions of the ice-water boundary during fountain on time steps.  $q_G$  quantifies the heat conduction process between the Icestupa surface layer and the ice body.

positive flux towards the surface of the icestupa are compensated by the net longwave radiation ( $-36 W m^{-2}$ ) and the melt energy ( $-19 W m^{-2}$ ). The contribution of other fluxes are negligible in comparison.

Net shortwave radiation is the main input to, and the most varying energy flux on the ice surface. Its variability is controlled by the surface albedo  $\alpha$  and the area fraction  $f_{cone}$  which therefore represent key variables in the energy balance (Fig. 7 (a)). Although global radiation flux reached a daily maximum value

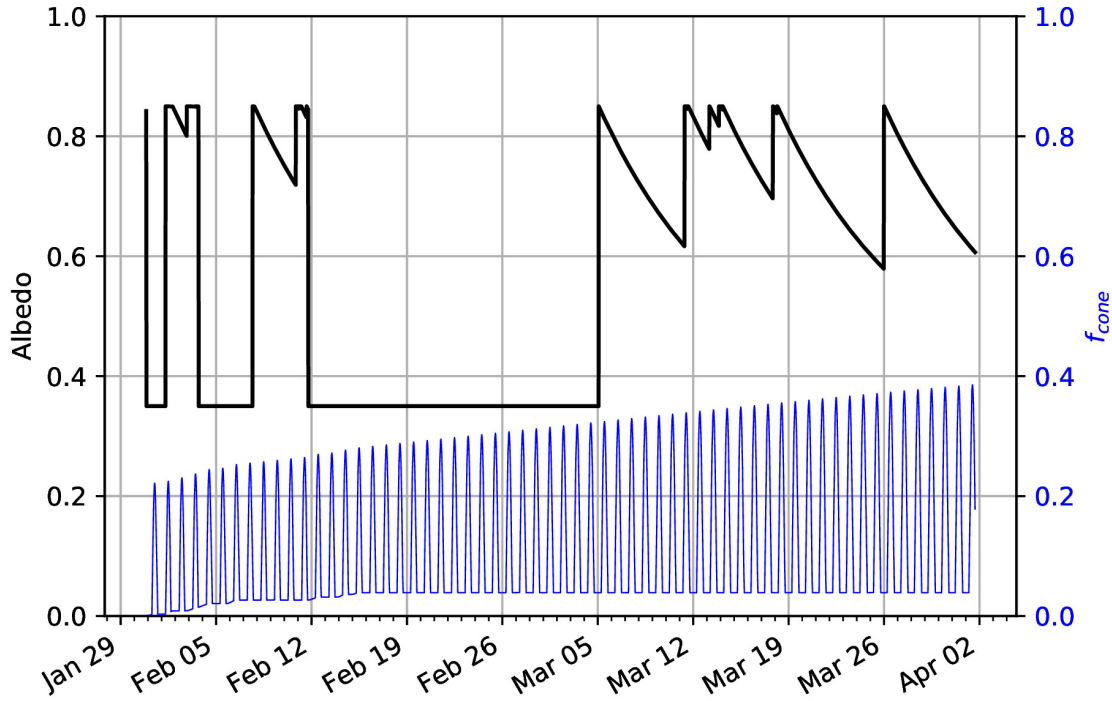


**Figure 7.** Some derived parameters of the model, namely, albedo and  $f_{cone}$  (a), Surface and bulk temperature (b). In (a), the black curve shows how snow and fountain-on events reset albedo between ice albedo and snow albedo. The decay of the snow albedo to ice albedo can also be observed. The blue curve shows how the solar radiation area fraction varied diurnally with variations in the solar elevation angle. In (b), the surface temperature (black curve) was forced to be  $0^{\circ}\text{C}$  during fountain activity. The corresponding bulk temperature is shown with the blue curve.

of  $304 \text{ W m}^{-2}$ ,  $q_{SW}$  only went up to  $68 \text{ W m}^{-2}$ . This is caused by the fact that only about 30 percent of the direct solar radiation influenced the Icestupa surface as shown by the area fraction  $f_{cone}$  in Fig. 7 (a). Snowfall is the atmospheric variable connected most closely and proportionally to albedo. Higher and/or more frequent snowfall thus decreases the energy available for melt due to the corresponding increase in  $\alpha$ .

$q_{LW}$  was predominantly negative indicating that this energy balance component drove the freezing of the ice structure. The incoming longwave radiation was strongly dependent on atmospheric emissivity which had a mean value of 0.77. Atmospheric emissivity in turn depended on the cloudiness factor. Daily values of  $q_{LW}$  ranged from -95 to  $7 \text{ W m}^{-2}$ .  $q_{LW}$  and  $q_S$  were both proportional to the temperature gradient between the air and the Icestupa surface. Turbulent sensible heat flux  $q_S$  contributed mostly to the melt of the ice structure. Daily values of  $q_S$  ranged from -16 to  $59 \text{ W m}^{-2}$ . Turbulent latent heat flux  $q_L$  was predominantly positive suggesting that it favoured deposition/condensation over evaporation/sublimation. Daily values of  $q_L$  ranged from -4 to  $47 \text{ W m}^{-2}$ . Therefore, the Icestupa gained mass cumulatively from the atmosphere due to the deposition/condensation process. Fountain water heat flux  $q_F$  had a mean of zero as it was only nonzero during 1002 time steps or around 100 hours. Daily values of  $q_F$  ranged from 0 to  $7 \text{ W m}^{-2}$ . The contribution of heat flux by conduction  $q_G$  was minimal as it only varied between -7 to  $7 \text{ W m}^{-2}$  with a mean of  $0 \text{ W m}^{-2}$ . The energy contributing to surface temperature changes ( $q_T$ ) was insignificant in comparison to the energy spent on freezing and melting ( $q_{melt}$ ). The resulting bulk temperature and the surface temperature are shown in Fig. 7 (b). For the total considered period,  $q_{LW}$  accounted for 28.3% of overall energy turnover. The energy turnover is calculated as the sum of energy

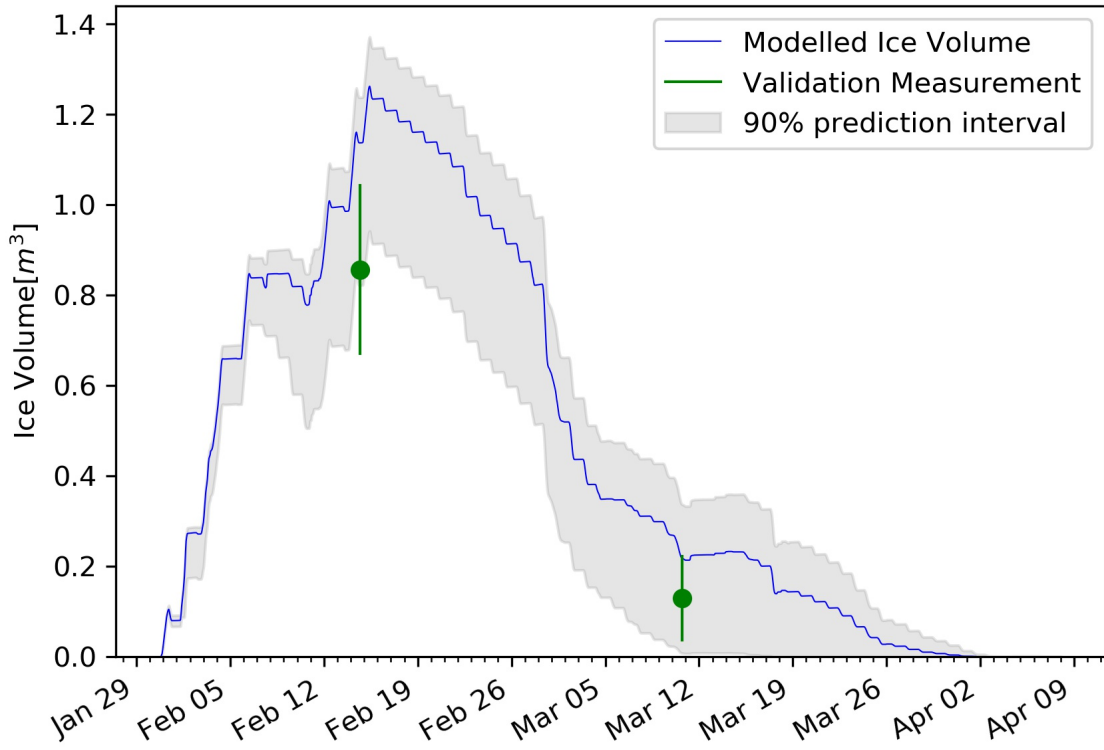


**Figure 8.** Modelled ice volume during the lifetime of the Schwarzsee Icestupa (blue curve). Green line segments indicate the first and second validation measurements. The prediction interval is based on the ice volume uncertainty caused by the most sensitive parameters, namely, temperature threshold below which precipitation falls as snow and the ice emissivity.

285 fluxes in absolute values.  $q_{SW}$  accounted for 21.7%, followed by  $q_{melt}$  (25.4%),  $q_S$  (14.6%),  $q_L$  (7.5%),  $q_G$   
286 (1.8%),  $q_F$  (0.3%) and  $q_T$  (0.3%).

287 Fig. 6 (b) represents the mass fluxes associated with these energy exchanges expressed in  $m$  w.e. It  
288 shows the ice and meltwater formed due to  $q_{melt}$ , snow accumulated due to precipitation, water vapour  
289 deposition/condensation and sublimation/evaporation due to  $q_L$ . Growth rate ( $\frac{\Delta M_{ice}}{\Delta t}$ ) shows a strong  
290 correlation with net energy flux ( $r^2 = 0.44$ ) but poor correlation with Icestupa surface area ( $r^2 = 0.04$ ).  
291 This is because the variance in growth rate is mostly due to the variance in  $q_{net}$  as illustrated in Fig. 6.  
292 Since  $r_{ice}$  was initialised with the spray radius  $r_F$ , the surface area maintains a maximum initially until the  
293 energy flux becomes positive. This trend favours the positive over the negative thickness changes resulting  
294 in a steep increase and gradual melting of ice volume as can be seen in Fig. 8.

295 The total water used for the Icestupa development includes contributions from the fountain (97.2%),  
296 snowfall (2.5 %) and deposition/condensation (0.3 %) as shown in Table 2. The maximum ice mass during  
297 the whole measurement period was 1158 kg, which occurred after the last fountain run on Feb 16<sup>th</sup> in the  
298 morning. Therefore, in the case of Schwarzsee we used a water input of 18,584 kg, with a resultant storage  
299 efficiency of only 7.5 %.

## 5 MODEL SENSITIVITY AND UNCERTAINTY ANALYSIS

300 The icestupa model can be regarded as a function  $f(x_1, x_2 \dots, x_n) = (y_1, y_2 \dots, y_m)$ , where  
301  $(x_1, x_2 \dots, x_n)$  are the model parameters and  $(y_1, y_2 \dots, y_m)$  are the model outputs. The influence of each

parameter on the output variables of interest were quantified and the most important physical parameters for the subsequent uncertainty analysis were determined. The sensitivity of a parameter  $x_j$  is determined by keeping all other parameters  $x_i, i \neq j$  fixed at their baseline value and varying  $x_j$  within values that are physically plausible.

A sensitivity study on the parameters (listed in Table 1) was performed with the maximum ice volume as the target variable. All the parameters were assumed to be independent of each other with a uniform distribution. This assumption ignores the auto-correlation present among the parameters associated with the albedo parameterisation. The range of uncertain parameters were set based on available literature values or varied  $\pm 5\%$  from the base value if no such reference was available. The uncertainty of all the site parameters were caused due to parallax errors during manual measurement. This was quantified with a range of  $\pm 1\%$  from the base value. However, it must be kept in mind that, even though intended to be as objective as possible, the selection of a parameter range has a subjective part that influences the results and conclusions obtained in this analysis. The variation of the model outputs  $y_k$  is evaluated to quantify the local sensitivities  $s_{j,k}$  that are defined here as the 95% range of the simulated outputs.

To perform the uncertainty analysis, we included only parameters that influence the maximum ice volume by at least  $0.1 m^3$ . All other parameters were fixed at their baseline value. Fig. 9 shows all the variance produced by these uncertain parameters in maximum ice volume calculation. It shows that  $\epsilon_{ice}$  and  $T_{rain}$  are the only parameters with a maximal sensitivity of more than  $0.1 m^3$  for the maximum ice volume estimate. Consequently, all other parameters were excluded from the subsequent uncertainty analysis.

The temperature threshold below which precipitation falls as snow ( $T_{rain}$ ) was found to be the most sensitive parameter. It is used in the model to reset the albedo to snow albedo and determine snow precipitation events. The lower  $T_{rain}$  parameter the higher the albedo (as the Icestupa surface has a lower albedo when ice-covered than when snow-covered). The variation of  $T_{rain}$  by 5% caused maximum ice volume variation of  $1.2 \pm 0.2 m^3$ .

Ice emissivity was also found to be a sensitive parameter. The higher the ice emissivity the larger the maximum ice volume as the emitted longwave radiation increases with ice emissivity. Variation of  $\epsilon_{ice}$  by 5% caused a maximum ice volume range from  $1.3 \pm 0.1 m^3$ .

In total, the sensitivity analysis required 120 simulations, and the uncertainty analysis a total of 32 simulations.

## 6 DISCUSSION

### 6.1 Model validation quality

We first evaluate the model against the validation measurements at the Schwarzsee site. The uncalibrated model is able to capture both the freezing and the melting process sufficiently well as the modelled ice volume lies within the uncertainty of both validation measurements. Furthermore, the validation measurements fit well within the estimated model uncertainty. However, since this validation is based on only two points, it does limit the confidence in the model results. Moreover, the model seems to overestimate the ice volume at both validation points. This could be due to the underestimation of the surface area which underestimates the melt rates (absolute growth rate when  $\frac{\Delta M_F}{\Delta t} < 0$ ) and the freeze rates (absolute growth rate when  $\frac{\Delta M_F}{\Delta t} > 0$ ). However, as the fountain was mostly inactive during the study period, the underestimation of surface area disproportionately undervalues the melt rates over the freeze rates. One major cause of this underestimation was the conical shape assumption, as in reality, the Icestupa shape ranged between a cone and a cylinder (Fig. 2). Another cause was the surface irregularities that

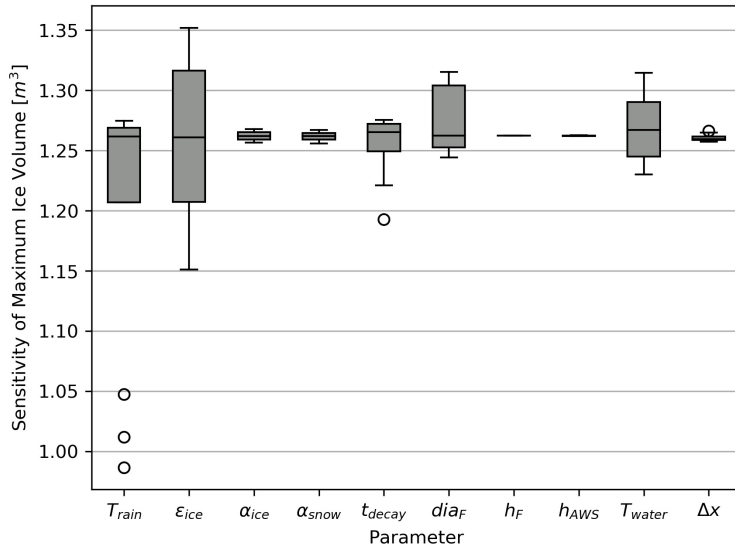


**Figure 9.** Sensitivities of maximum ice volume to all the uncertain and site parameters used in the model (Table 1). Outliers in the bar plot are shown as 'o'.

were observed due to uneven exposure to direct solar radiation and fountain droplets. The sensitivity of the model results to these errors was further amplified due to the relatively small volume of the Schwarzsee Icestupa. In summary, more validation measurements on a more voluminous Icestupa would have increased confidence on the model results.

## 6.2 Important assumptions

In the sensitivity and uncertainty analysis presented above, we did not account for several general assumptions and parametrisation choices that may cause model errors. Some assumptions and their potential to cause errors are discussed below.

- Turbulent Sensible and Latent Heat Fluxes: The method used to calculate the turbulent heat fluxes by Garratt (1992) assumes that the turbulent heat fluxes are acting over a uniform planar surface to determine the roughness length. Since our application is on a conical surface,  $z_{ice}$  has no real physical significance.
- Droplet flight time loss: Water losses during the flight time of fountain droplets were neglected making all the fountain spray available for freezing. For the Schwarzsee experiment, inclusion of this parameter does not influence results since it is already accounted for in the drained water discharge rate which was at least  $3 \text{ l min}^{-1}$ .
- Nucleation of droplets: Corresponding to droplet flight time, ice/snow formation is also possible before surface contact if nucleation occurs during flight time. For the Schwarzsee experiment, this process will further increase the freeze rate and hence the storage efficiency. This process is neglected for model simplicity.

## 6.3 Schwarzsee vs Ladakh Icestupa

It could be argued that the relatively small Schwarzsee Icestupa cannot be compared with the much larger Icestupas in Ladakh which store millions of litres of water for several months (see Appendix 8.1). However, this is the only Icestupa dataset available for such a model validation.

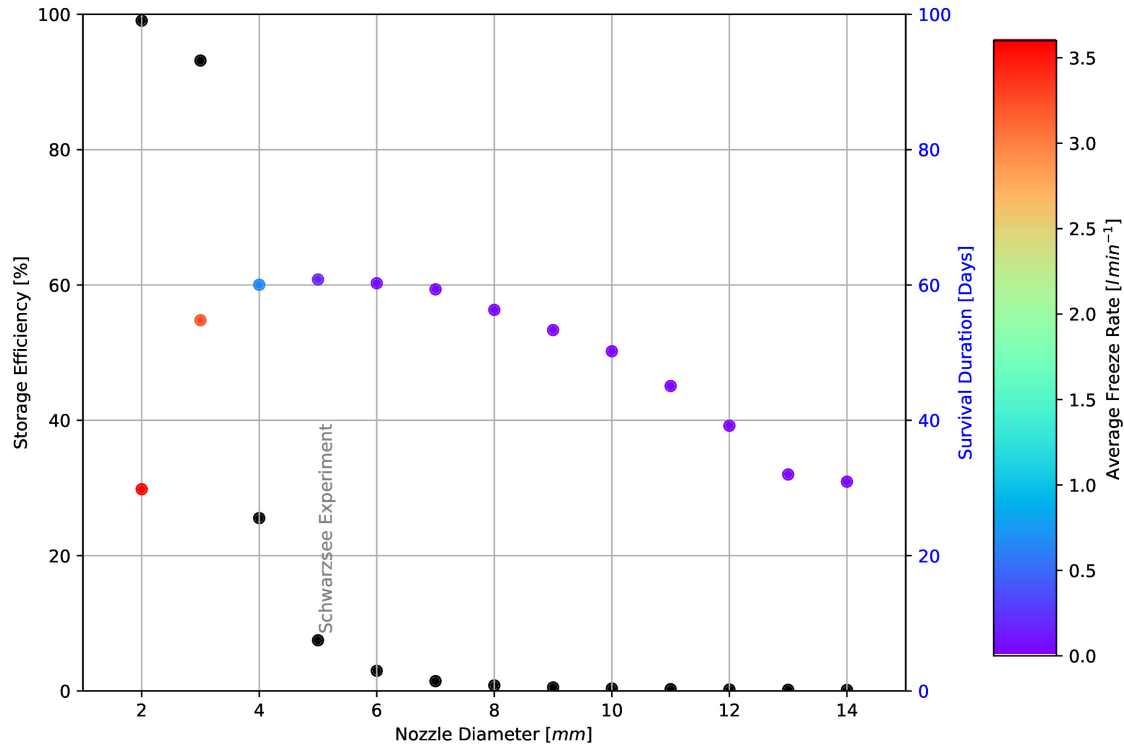


**Figure 10.** Variation in storage efficiency (black dots) and storage duration (coloured dots) with changes in fountain nozzle's nozzle diameter. The dot colours represent average freeze rate based on the color bar.

367 Table 2 clearly shows that for our Schwarzsee experiment most of the input water (92 %) simply drained  
 368 away. This high water loss through drainage is due to the fact that the average spray rate of the fountain  
 369 ( $(\frac{\Delta M_F}{\Delta t})_{mean} = 3.6 \text{ l min}^{-1}$ ) far exceeded the max Icestupa growth rate ( $(\frac{\Delta M_{ice}}{\Delta t})_{max} = 1 \text{ l min}^{-1}$  (w.e.) ).

370 In the city of Leh, Ladakh at an altitude of 3500 m a.s.l. the air temperature shows values down to  
 371  $27.9^\circ\text{C}$  in winter (Chevuturi et al., 2018) whereas Schwarzsee had a minimum temperature of just  $-11.6^\circ\text{C}$   
 372 during the study period. Moreover, subzero temperatures were only reached for 7 nights of fountain  
 373 operation at the Schwarzsee site compared to the 43 nights of fountain operation possible in Ladakh (see  
 374 Appendix 8.1). Thus, the Icestupa growth rate is expected to be much higher in Ladakh. However, water  
 375 spray rates in Ladakh are also much higher (around  $210 \text{ l min}^{-1}$ ). So the water losses in Ladakh could  
 376 also be caused due to excessive fountain spray.

#### 377 6.4 Icestupa construction decisions

378 There are several decisions one has to take when constructing Icestupas. These can be broadly divided  
 379 into two types of decisions, namely fountain and location decisions. Both the meteorological conditions  
 380 of the location and the surface area produced by the fountain significantly influence the observed growth  
 381 rate. Since our validation is restricted to just one location, we restrict our discussion to the optimization  
 382 possibilities of Icestupa constructions through fountain decisions.

383 Assuming a constant spray for the fountain, we can divide the fountain decisions into fountain state  
 384 (on/off) and type (height and nozzle diameter). From an energy balance point of view, the fountain should  
 385 be switched on for all time intervals when  $q_{net} < 0$ . However, in our experiment, the fountain state decision  
 386 was set based on whether the ambient temperature was above or below a critical temperature of  $-5^\circ\text{C}$ .  
 387 Ambient temperature can serve as an indicator of  $q_{net}$  as it was correlated ( $r^2 = 0.53$ ). However,  $q_{net}$

388 was found to be negative already at a critical temperature of  $-1^{\circ}\text{C}$ . Therefore, using air temperature to  
389 determine when the fountain should be switched on is justified but a higher critical temperature could have  
390 been used in the case of the Schwarzsee Icestupa.

391 The fountain type used can be characterised by the physical structure of the fountain, namely its height and  
392 nozzle diameter. Maintaining the same spray rate and height, one can optimize the Icestupa development  
393 by identifying the minimum nozzle diameter that yields the maximum storage efficiency.

394 Fig. 10 shows reducing the nozzle diameter to 3 mm increases storage efficiency up to 93 % without  
395 compromising much on storage duration. The corresponding storage quantity of the 3 mm nozzle diameter  
396 was more than 20 times higher than the 5 mm fountain used in our experiment. This is because the spray  
397 radius  $r_F$  of the 3 mm fountain was much higher at 8.5 m compared to the 1.7 m spray radius of the  
398 5 mm fountain (see Appendix Section ??). Here, we define growth rate as freeze rate when fountain is  
399 active and melt rate otherwise. So this higher spray radius both, increases the freeze rate and increases  
400 the melt rate since they are both directly proportional to the surface area. However, since the freeze rate  
401 cannot increase beyond a spray rate of  $3.6 \text{ l min}^{-1}$  (except during precipitation or deposition/condensation  
402 events), an optimum spray radius or nozzle diameter exists, beyond which storage duration suffers due to a  
403 disproportionate increase in melt rate compared to the freeze rate. So even though 3 mm nozzle diameter  
404 had a much higher storage quantity than the 5 mm nozzle, its storage duration was around 6 days lesser  
405 than the 5 mm nozzle. One physical cause of this effect is the different shapes of both the ice structures. A  
406 flat sheet of ice (effectively a cone with a high spray radius) with higher mass might have a storage duration  
407 shorter than a conical ice structure. As the spray radius decreases with increasing nozzle diameter, the ice  
408 structure's average slope increases and so the 5 mm nozzle's ice structure is "more" conical than the 3 mm  
409 ice structure. Fig. 10 shows that a nozzle diameter of 3 mm has an average freeze rate ( $3.2 \text{ l min}^{-1} \text{ w.e.}$ )  
410 which is large enough to increase the storage efficiency and small enough to not reduce the storage duration  
411 of the Icestupa significantly.

## 7 CONCLUSIONS

412 We have outlined a methodology for estimating ice, liquid water, water vapour and drained quantities  
413 produced during the construction of an Icestupa using measurements of fountain spray rate, air temperature,  
414 radiation, humidity, pressure, wind and cloudiness at the Schwarzsee study site. The comparison with  
415 validation measurements at two different dates during the experiment led to satisfying results, although a  
416 more rigorous model validation was not possible due to few icestupa volume measurements.

417 According to the model, the Schwarzsee Icestupa achieved a storage quantity of 1392 litres of water with  
418 a storage duration of 61 days. However, the corresponding storage efficiency was very low with only 7.5 %  
419 for a water input of 18,584 litres. These estimates were most sensitive to the temperature threshold that  
420 determined precipitation phase and ice emissivity parameters which created an uncertainty of  $1.2 \pm 0.3 \text{ m}^3$   
421 in the maximum ice volume calculated. This is to be expected as net longwave radiation and net shortwave  
422 radiation together accounted for around 50 % of the overall energy turnover.

423 Although the location, storage quantity and duration of our experimental Schwarzsee Icestupa are not  
424 representative of the much larger Icestupas of Ladakh, the model results do support the hypothesis that  
425 there could be considerable water loss during the formation of Icestupas particularly due to excessive  
426 fountain spray. Using model calculations, it was shown that a decreased fountain nozzle diameter of 3 mm  
427 can increase the storage efficiency drastically. This is because a change in the fountain nozzle diameter  
428 causes an effective change of the ice surface area over which the net energy flux can act. This result has  
429 relevance on the future design of Icestupa fountains. However, care has to be taken as our model is currently

430 only validated by one experiment at the Schwarzsee site. Further experiments at different locations with  
431 different fountains are required to better understand the influence of construction decisions on the results.

## 8 APPENDIX

### 432 8.1 Ladakh Icestupa 2014/15

433 A 20 m tall Icestupa (Wangchuk, 2015c) was built in Phyang village, Ladakh at an altitude of 3500  
434 m a.s.l. Assuming a conical shape with a diameter of 20 m, the corresponding volume of this Icestupa  
435 becomes 2093 m<sup>3</sup> or 1,919,587 litres w.e. The fountain sprayed water at a rate of 3.5 l s<sup>-1</sup> (Wangchuk,  
436 2015e) from 21<sup>st</sup> January (Wangchuk, 2015a) to at least until 5<sup>th</sup> March 2015 (Wangchuk, 2015b) (around  
437 43 nights). Assuming fountain spray was active for 8 hours each night, we estimate water consumption to  
438 be around 4,334,400 litres. So just during construction/freezing period of the Icestupa, roughly 56 % of the  
439 water provided was wasted. The actual water loss is bound to be much higher due to further vapour losses  
440 during the melting period. This Icestupa completely melted away on 6<sup>th</sup> July 2015 (Wangchuk, 2015d).  
441 Therefore, the storage duration was 166 days or roughly 5 months.

## CONFLICT OF INTEREST STATEMENT

442 The authors declare that the research was conducted in the absence of any commercial or financial  
443 relationships that could be construed as a potential conflict of interest.

## AUTHOR CONTRIBUTIONS

444 SB wrote the initial version of the manuscript. MH, ML, SW, JO, and FK commented on the initial  
445 manuscript and helped improve it. SB developed the methodology with inputs from MH. SB performed the  
446 analysis with support from MH and ML. SB and MH participated in the fieldwork.

## FUNDING

447 This work was supported and funded by the University of Fribourg and by the Swiss Government Excellence  
448 Scholarship (Suryanarayanan Balasubramanian).

## ACKNOWLEDGMENTS

449 We thank Mr. Adolf Kaeser and Mr. Flavio Catillaz at Eispalast Schwarzsee for their active participation  
450 in the fieldwork. We would also like to thank Digmesa AG for subsidising their flowmeter used in the  
451 experiment. We would particularly like to thank the editor Prof. Thomas Schuler who gave us important  
452 inputs to improve the paper and we thank also Prof. Christian Hauck and Prof. Nanna B. Karlsson for  
453 valuable suggestions that improved the manuscript.

## DATA AVAILABILITY STATEMENT

454 The data and code used to produce results and figures will be published at a later stage and can, until then,  
455 be obtained from the authors upon request.

## REFERENCES

456 Apel, H., Abdykerimova, Z., Agalhanova, M., Baimaganbetov, A., Gavrilenko, N., Gerlitz, L., et al. (2018).  
457 Statistical forecast of seasonal discharge in central asia using observational records: development of a  
458 generic linear modelling tool for operational water resource management. *Hydrology and Earth System  
459 Sciences* 22, 2225–2254. doi:10.5194/hess-22-2225-2018

- 460 Bonales, L. J., Rodriguez, A. C., and Sanz, P. D. (2017). Thermal conductivity of ice prepared under  
461 different conditions. *International Journal of Food Properties* 20, 610–619. doi:10.1080/10942912.  
462 2017.1306551
- 463 Brutsaert, W. (1975). On a derivable formula for long-wave radiation from clear skies. *Water Resources  
464 Research* 11, 742–744. doi:10.1029/WR011i005p00742
- 465 Brutsaert, W. (1982). *Evaporation into the Atmosphere. Theory, History and Application* (Kluwer Academic  
466 Publishers)
- 467 Buytaert, W., Moulds, S., Acosta, L., Bievre, B. D., Olmos, C., Villacis, M., et al. (2017). Glacial melt  
468 content of water use in the tropical andes. *Environmental Research Letters* 12, 114014. doi:10.1088/  
469 1748-9326/aa926c
- 470 Chen, Y., Li, W., Deng, H., Fang, G., and Li, Z. (2016). Changes in central asia's water tower: Past, present  
471 and future. *Nature* doi:10.1088/1748-9326/aa926c
- 472 Chevuturi, A., Dimri, A. P., and Thayyen, R. J. (2018). Climate change over leh (ladakh), india. *Theoretical  
473 and Applied Climatology* 131, 531–545. doi:10.1007/s00704-016-1989-1
- 474 [Dataset] Copernicus Climate Change Service (C3S) (2017). Era5: Fifth generation of ecmwf atmospheric  
475 reanalyses of the global climate
- 476 Cuffey, K. M. and Paterson, W. S. B. (2010). *The Physics Of Glaciers* (Elsevier)
- 477 Fujita, K. and Ageta, Y. (2000). Effect of summer accumulation on glacier mass balance on the  
478 tibetan plateau revealed by mass-balance model. *Journal of Glaciology* 46, 244–252. doi:10.3189/  
479 172756500781832945
- 480 Garratt, J. R. (1992). *The Atmospheric Boundary Layer* (Cambridge University Press)
- 481 Grossman, D. (2015). As himalayan glaciers melt, two towns face the fallout
- 482 Hock, R., Rasul, G., Adler, C., Cáceres, B., Gruber, S., Hirabayashi, Y., et al. (2019). 2019: High mountain  
483 areas. *IPCC Special Report on the Ocean and Cryosphere in a Changing Climate* [H.-O. Pörtner, D.C.  
484 Roberts, V. Masson-Delmotte, P. Zhai, M. Tignor, E. Poloczanska, K. Mintenbeck, A. Alegria, M. Nicolai,  
485 A. Okem, J. Petzold, B. Rama, N.M. Weyer (eds.)]
- 486 Hoelzle, M., Barandun, M., Bolch, T., Fiddes, J., Gafurov, A., Muccione, V., et al. (2019). *The status and  
487 role of the alpine cryosphere in Central Asia*. doi:10.4324/9780429436475-8
- 488 [Dataset] IDAWEB (2019). Meteoswiss, federal office of meteorology and climatology
- 489 Immerzeel, W. W., Lutz, A. F., Andrade, M., Bahl, A., Biemans, H., Bolch, T., et al. (2019). Importance  
490 and vulnerability of the world's water towers. *Nature* 577, 364 – 369. doi:10.1038/s41586-019-1822-y
- 491 Meteoblue (2020). Climate schwarzsee
- 492 Mölg, T. and Hardy, D. R. (2004). Ablation and associated energy balance of a horizontal glacier surface  
493 on kilimanjaro. *J. Geophys. Res.-Atmos.* 109, 1–13. doi:10.1029/2003JD004338
- 494 Nüsser, M., Dame, J., Kraus, B., Baghel, R., and Schmidt, S. (2019a). Socio-hydrology of artificial glaciers  
495 in ladakh, india: assessing adaptive strategies in a changing cryosphere. *Regional Environmental Change*  
496 doi:10.1007/s10113-018-1372-0
- 497 Nüsser, M., Dame, J., Parveen, S., Kraus, B., Baghel, R., and Schmidt, S. (2019b). Cryosphere-Fed  
498 Irrigation Networks in the Northwestern Himalaya: Precarious Livelihoods and Adaptation Strategies  
499 Under the Impact of Climate Change. *Mountain Research and Development* 39. doi:10.1659/  
500 MRD-JOURNAL-D-18-00072.1
- 501 Oerlemans, J. and Knap, W. H. (1998). A 1 year record of global radiation and albedo in the  
502 ablation zone of morteratschgletscher, switzerland. *Journal of Glaciology* 44, 231–238. doi:10.  
503 3189/S0022143000002574

- 504 Schmidt, L. S., Aðalgeirsdóttir, G., Guðmundsson, S., Langen, P. L., Pálsson, F., Mottram, R., et al. (2017).  
505 The importance of accurate glacier albedo for estimates of surface mass balance on vatnajökull: evaluating  
506 the surface energy budget in a regional climate model with automatic weather station observations. *The  
507 Cryosphere* 11, 1665–1684. doi:10.5194/tc-11-1665-2017
- 508 Stigter, E. E., Litt, M., Steiner, J. F., Bonekamp, P. N. J., Shea, J. M., Bierkens, M. F. P., et al. (2018).  
509 The importance of snow sublimation on a himalayan glacier. *Frontiers in Earth Science* 6, 108.  
510 doi:10.3389/feart.2018.00108
- 511 Unger-Shayesteh, K., Vorogushyn, S., Farinotti, D., Gafurov, A., Duethmann, D., Mandychev, A., et al.  
512 (2013). What do we know about past changes in the water cycle of central asian headwaters? a review.  
513 *Global and Planetary Change* 110, 4 – 25. doi:10.1016/j.gloplacha.2013.02.004. Water in Central Asia  
514 – Perspectives under global change
- 515 Wangchuk, S. (2014). Ice stupa artificial glaciers of ladakh
- 516 Wangchuk, S. (2015a). The good news at ice stupa 24th january 2015
- 517 Wangchuk, S. (2015b). Ice stupa artificial glacier inaugurated 5th of march 2015
- 518 Wangchuk, S. (2015c). Ice stupa surpasses guiness world record
- 519 Wangchuk, S. (2015d). Ice stupa way of celebrating a special day
- 520 Wangchuk, S. (2015e). World water day at ice stupa
- 521 WMO (2018). *Guide to Instruments and Methods of Observation* (World Meteorological Organization ;  
522 2018 (2018 Edition))
- 523 Woolf, H. M. (1968). *On the Computation of Solar Elevation Angles and the determination of sunrise and  
524 sunset times* (National Aeronautics and Space Administration)
- 525 Zhou, S., ShiQiao nd Kang, Gao, T., and Zhang, G. (2010). Response of zhadang glacier runoff in nam  
526 co basin, tibet, to changes in air temperature and precipitation form. *Chinese Science Bulletin* 55,  
527 2103–2110. doi:10.1007/s11434-010-3290-5